

An Image Analogies Approach for Multi-Scale Contour Detection

Slimane Larabi¹, Neil M. Robertson²

¹ Computer Science Department, USTHB University,

² Queen's University of Belfast

Contents

1	Introduction	3
1.1	Contributions	4
1.2	Paper roadmap	5
2	Image Analogies for Contour Detection: A Naive Application	7
3	The basic principle of our method	9
3.1	The best approximate match	10
3.2	The best coherence match	11
4	Making the Training Images	11
4.1	Duality of the two sets of artificial patterns	16
4.2	Obtaining of most significant outline	17
5	Algorithm, Complexity and Details of the Implementation	19
6	Results	21
6.1	New benchmarks for BSD 500 dataset	21
6.2	Parameter settings	21
6.3	Using hand-drawn contours as training images	23
6.4	Using pairs of artificial patterns as training images	25
6.5	Contour detection at different levels of resolution	27
6.6	Affine transformation Invariance	27
7	Evaluation and Discussion	30
7.1	Visual estimating of the quality of contour detection: some samples . . .	31
7.2	Evaluating contour detection quality on BSD500 data set	33
7.3	Evaluating contour detection quality on Weizmann Horses data set . . .	34
7.4	Discussion	35

2 *An Image Analogies Approach for Multi-Scale Contour Detection*

8 Conclusion **36**

8.1 Further work 37

9 Appendix: Constraints required for images training **37**

1 Introduction

Contour detection is an important task in many computer vision applications such as object recognition, motion, medical image analysis, image enhancement and image compression.

Several authors define contours as the boundaries of objects in an image. This definition would exclude many situations in which contours do not arise from region boundaries (38).

We agree with G. Papari and N. Petkov (38) considering that concept of contour is broader than the concept of region boundary and human judgment is the only possible criterion that can be used in order to say if a given visual feature is a contour or not. Contours are then defined in a given image as the set of lines that human observers would consent on to be the contours in that image.

There is wide range of methods in the literature devoted to contour detection (55), (23), (48), (24) (38). The main problem that has been dealt with in the literature is the modelling of the contour pixel.

The first approaches proposed to contour detection are based on local measurements in image. Local derivative filters have been proposed by Roberts (45), Sobel (18), and Prewitt (42). In the next, Marr and Hildreth (34) proposed the use of zero crossings of the Laplacian of Gaussian operator. The Canny detector (9) also models contours as sharp discontinuities in the brightness channel, adding non-maximum suppression and hysteresis thresholding steps and became the most popular differential operator. Many algorithms have been proposed using others filters (37), (22), (40) or for locating contour of texture (28), (13), (47).

Instead of searching for points where there are sharp changes in intensity, local energy and phase congruency have been used in many algorithms for contour detection and feature extraction (30), (40), (43), (44), (50), (46). Other important techniques proposed for contour detection concerns active contours methods. Initially proposed by Kass et al (29), this work has been improved tacking into account topology, distance and gradient vector flow (36), (14), (53). Other improvement are the Level set algorithm introduced by Malladi et al (33) which doesn't make assumption about the topology of the objects in the image and the geodesic active contour based on the relation between active contours and the computation of geodesics or minimal distance curves (10).

Contour detection has reached high degree of maturity, taking into account multimodal contour definition. However, the quality of located contours are still far from what people can do. This may arise from the missing of human knowledge (high level of vision) and human expertise to hand draw contours

(low level of vision) in the different proposed approaches.

Indeed, humans can do easily this and results are known to be very similar from person-to-person.

The aim of this work is to introduce image analogies in early stages of computer vision, to model human expertise and to pass it to the computer for contour detection. Indeed, image analogies constitutes a natural means of specifying filters and image transformations (26) and we can supply an appropriate exemplar and say, in effect, “Find me pixels which look like this”. The concept is illustrated in figure 1.

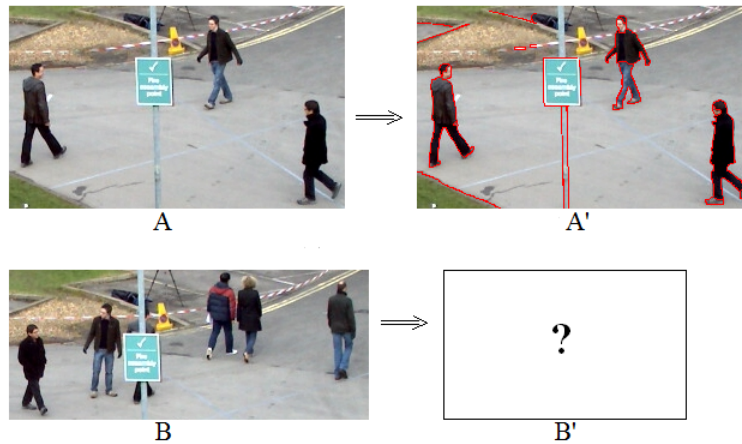


Figure 1: Contour detection by analogy: the basic principle proposed in this work is to use previously detected contours to find new ones in similar images: Given the pair of training images (A, A') where the contours in A are hand drawn, our aim is to locate the contours of a query image B in the same way that it has been done for A

1.1 Contributions

Our contributions are:

- First, Image analogies principle is applied naively to contour detection. Due to the high complexity of this task, a set of 14 artificial pairs of patterns $(P_i, P'_i, i = 1..14)$ are derived from a mathematical reasoning so that any contour pixel will be located whatever the lighting conditions in image. Contours located are related to regions boundaries and are in evolution from darker region to the clearer region (see figure 2) where located contours using 4 pairs of patterns are illustrated).



Figure 2: Contours located by respectively by the pairs of patterns (P_5, P'_5) , (P_6, P'_6) , (P_7, P'_7) , (P_8, P'_8)

- Contours are computed for a query image at different scales. At the low resolution only the low frequency (LF) contours are visible corresponding to large differences in intensity between regions. The more the resolution increases, the more there are contours corresponding to intermediate and high frequency (IF), (HF). Figure 3 shows computed contours by image analogies illustrating this point where the black, red, green are the color of contour pixels of level (LF), (IF) and (HF).

- Our method requires the fixing of three parameters whose values are known and the result of contours detection doesn't depend from any other parameter and are unique for all images.

1.2 Paper roadmap

In section 2, we present our approach for contour detection using image analogies principle. Based on stored information in the reference images, contour pixels in a query image are located applying image analogy technique. A naive



Figure 3: (a) A query image, (b) Contours of Low Resolution, (c) Contours of Intermediate Resolution, new located contours are illustrated with red color, (d) Contours of High Resolution, new located contours are illustrated with green color

application is proposed and the limits of this approach is explained. Indeed, it is necessary to have many reference images, otherwise some contour pixels will be not located in the new image since their appearance may not be represented in the training data. To deal with this constraint, we study in section 3 the required constraints for training images so that all contour pixels will be located for any query image. Artificial pairs of patterns are derived from this study and used as reference instead of real images. We explain in section 4 how these patterns are build. In section 5 we study the complexity of the proposed approach and we gives the improvements made for reducing this complexity. Some details of the implementation and the algorithm are given.

Different data sets including the Berkeley Segmentation Data (BSDS500) (3), Weizmann Horses (7) are used to validate this approach. Obtained results their evaluation are presented in Section 6. We conclude this paper with propositions for integrating image analogies at other stages of image analysis.

2 Image Analogies for Contour Detection: A Naive Application

A human is able to detect and draw natural image contours. Applying image analogies principle, our aim is to locate contours as accurately as a human does it, including within images of low resolution where objects have small sizes.

Let A be the initial image. We assume that contour pixels are manually located on A and marked giving a synthesized image A' (see figure 4 where pixels contours are highlighted with red colour). Given a query image B , the problem is then how to compute the synthesized image B' that contains contours located and highlighted in the same way as those located in A' . The key idea is to classify each pixel q of B using the knowledge that may be inferred from (A, A') : for each pixel q , the synthesized pixel q' will be the same pixel as q , in addition it will be marked contour pixel if the pixel p^* in A' associated to p^* in A is marked so as p^* is the best match of q . The similarity measure considered as Euclidean distance is computed taking into account the neighbours of q and p and concerns only the brightness of pixels.

In the case where the query image has the same background **like** the training pair of images (A, A') , the algorithm find almost all contour pixels because the best match p^* of a query contour pixel q will be found that it coincides with a marked pixel (see figure 4).



Figure 4: (Left) First training pair (A_1, A'_1) where drawn pixel contours are highlighted with red color in A'_1 , (Right) Query image B_1 and the computed image B'_1

The naive application of image analogies for contour detection has been our first task: we found that this method does not work. Figure 5 shows an example where the training images pair is not sufficient to locate all contour pixels in the query images because its brightness is completely different from that of the images training. However, if we increase the number of learning images, this will increase the probability to match correctly query pixels, and then the result of image analogies may be better if there are similarity between query image

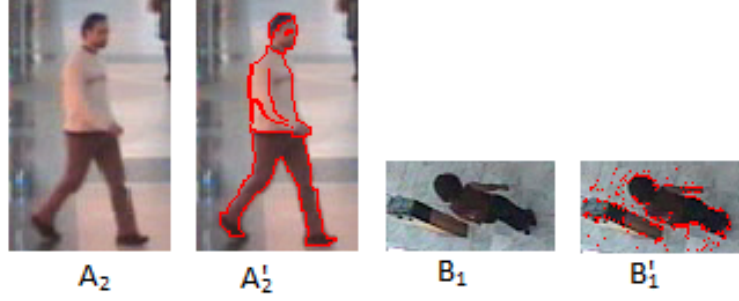


Figure 5: (Left) Second training pair A_2, A'_2 with different brightness than the first one, (Right) For the same query image B_1 , the computed B'_1 where many contour pixels are not located



Figure 6: A third and fourth training images pair $(A_3, A'_3), (A_4, A'_4)$



Figure 7: From the left to right: the computed B'_2 for a second query image B_2 respectively using (first), (first and third), (first, third and fourth) training images pairs. We note the increasing of located contour pixels when more training images related to the query image are used

and some reference images (see figures 6, 7). This way to improve the quality of contour detection implies a considerable increasing of time processing.

When the query images are of the same nature as the training images, the results may be good. This is the case in (31), image segmentation is done in this work applying directly image analogies technique in particular case of set of consecutive Visible Human slices: m_0, m_1, \dots, m_n . Given a human segmented

image s_0 , Image Analogies is applied firstly using the same segmented s_0 for all m_i and progressively for s_i , the computed segmented image s_{i-1} is used. The performance is improved significantly: If other query image m_i (different from the slices) is used, the result of image analogies will depend on the texture, color of the regions contained in image m_0 . If m_i and m_0 are different, poor segmentation will be obtained. This is due to the step of pixel matching between m_i and m_0 . If we cannot find for a query pixel q in m_i a good match p in m_0 , then the pixel q in s_i will be misclassified.

We investigated in this work, how can we avoid this constraint (more learning images are required) in order to guarantee that all contour pixels will be located for any query image. This limitation may be avoided using many pairs of training images in different conditions of illumination. This will increase the processing time and also it is a hard task to acquire sufficient manually-labelled data. In the next section, we propose a new way to deal with this limitation which allows independence from the task of obtaining manually-located outlines.

3 The basic principle of our method

Before the describing of the proposed method, we discuss the scope of human expertise for contour detection. Given an image A , we believe that the human takes into account two criteria for locating contours. The first one is the neatness of the difference of gray level intensity (or colour) between two neighboring sets of pixels. The second one is the knowledge of outline shape geometry inferred from context or some features such as outlines of dominant parts (16). Indeed, during the process of outline drawing, a human cannot localize some parts of the outline due to the high similarity between pixels of background and object part but can avoid this difficulty using the prior knowledge (see figure 8).

In this paper we deal only with the first criterion and we present our approach in order to allow computer locating contour pixels in similar way that human do. We model hand drawing contours, using only the brightness feature.

Let (A, A') be pair of training images such that A' be the synthesized image identical to A , in addition contour pixels are marked. Let B be a query image. Applying image analogies principle means that for each pixel q of B , its best match p^* is searched in A using:

- The brightness similarity between the neighbors of p and q (**best approximate match**).
- The selected p^* must verify the **best coherence match**, which means if the



Figure 8: Initial image A and the synthesized image A' obtained as A in addition contour pixels are marked (illustrated with red color). Note here that the difficulty to locate contours in such images of low-resolution is due to the similarity of the background and some parts of objects

neighbors of q are pixels of contours, it will be also the case for the neighbors of the selected p^* .

3.1 The best approximate match

Let $N(p)$, $N(q)$ be the $(m \times m)$ neighborhood of p, q in images A, B . Our aim is to search in A the best match $N(p^*)$ of $N(q)$. The similarity measure $S(q, p)$ between $N(q)$ and $N(p)$, given by equation 1, is computed as the Euclidian distance between the intensities of corresponding pixels in $N(q)$ and $N(p)$ (see figure 9).

$$S(q, p) = \sum_{u=-w}^{u=+w} \sum_{v=-w}^{v=+w} (N(q)(i+u, j+v) - N(p)(k+u, l+v))^2 \quad (1)$$

Where:

1. $(i, j), (k, l)$ are the coordinates of the pixels q, p in images B, A
2. $N(q)(i+u, j+v)$, $N(p)(k+u, l+v)$ are the intensities of pixels $(i+u, j+v)$ and $(k+u, l+v)$ in images B, A .
3. $m \times m$ is the size of $N(p)$ and $N(q)$ and $w = (m - 1)/2$

The proposed similarity measure must guarantee that any pixel q cannot be misclassified if the knowledge inferred from (A, A') is sufficient.

Based on the proposed similarity measure, we study in annex 9 the necessary constraints that must be verified in the training images (A, A') in order to guarantee that all contour pixels and only contour pixels will be selected.

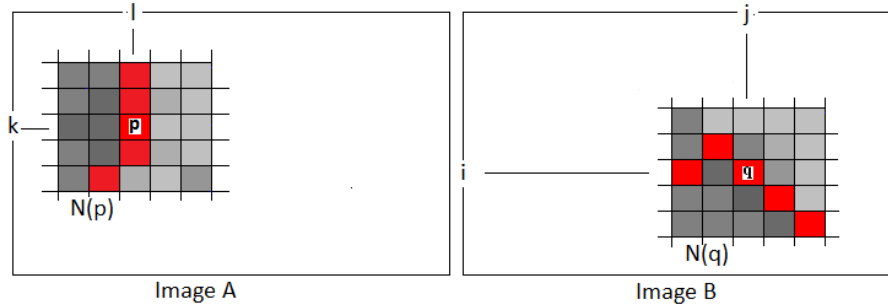


Figure 9: Example of two neighbors $N(p), N(q)$, in red color boundary pixels

3.2 The best coherence match

This criterion is considered in order to favour the matching of aligned pixel contours in both neighboring $N(q), N(p)$. Then, in addition to the lighting conditions, it is necessary to have all directions of contours pixels in the training images. We consider then the presence of n directions of contours in A, A' . For example if $n = 4$ (see figure 10), the directions are horizontal, vertical and the two diagonals directions are considered.

Considering these occurrences in the training images, any query $N(q)$ will be matched with $N(q)$ having the same direction of the boundary and nearest intensities corresponding to the minimal value of the similarity measure.

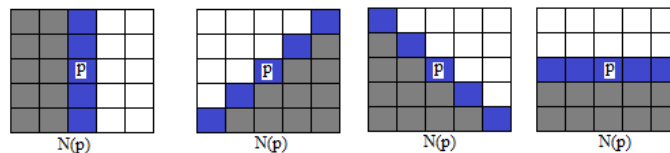


Figure 10: Case of four directions of the boundary in $N(p)$, in blue color are represented contour pixels

4 Making the Training Images

From the conducted study presented in annex 9 devoted to the constraints required for the pairs of training images, there are some constraints that must be verified in the image A in order to ensure that all q outline pixels will be correctly classified, otherwise, the contour pixel q will be misclassified.

Two constraints on the value of d_A must be verified (see annex 9):

if $d_A > 0$:

$$2d_b + 2 \triangle I_A^b < d_A < 2d_B + 2d_b - 2 \triangle I_A^b \quad (2)$$

if $d_A < 0$:

$$2d_B + 2d_b + 2 \triangle I_A^b < d_A < 2d_b \quad (3)$$

Case 1

Our goal is to have in A the located contour pixels which verify for each $N(p)$:

$$d_A \in]2d_b + 2 \triangle I_A^b, 2d_G + 2d_B - 2 \triangle I_A^b[\quad (4)$$

This interval depends on the image B , particularly on the values I_B^b, I_B^f of each $N(q)$.

It is unrealistic to have all possible pairs of images (A, A') whose located contour pixels verify the constraint given by the equation 2 for all pixels q of any B image.

What we propose here is to use artificial images (A, A') which allow to have for any $N(q)$ the constraint satisfied.

Consequently, we assume that I_A^b, I_A^f are fixed values in $N(p)$, where p is a contour pixel. Then, the values of I_B^b, I_B^f satisfying the equation 2 correspond respectively to $I_B^{b*} = (I_A^f - \varepsilon - I_A^b)/2$, and any value of I_B^f greater than $I_B^b + \delta l$, where ε is a smallest intensity ($\varepsilon = 1$) and δl is the smallest difference of intensity between two regions (see figure 11). Then any $N(q)$ with these values of I_B^b, I_B^f verifies the equation 2 and the pixel q will be classified correctly using $N(p)$.

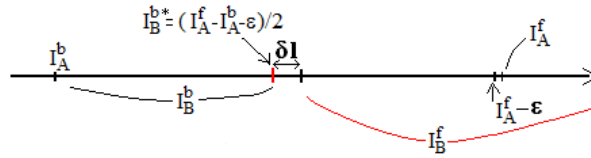


Figure 11: For given values (I_A^b, I_A^f) of $N(p)$, all $N(q)$ such that $I_B^b < I_B^{b*}$ and $I_B^f \geq I_B^{b*} + \delta l$ satisfy the equation 2

In addition, all (I_B^b, I_B^f) of $N(q)$ so as $I_A^b < I_B^b \leq I_B^{b*}$ and $I_B^f \geq I_B^{b*} + \delta l$ verify the equation 2. Indeed, if I_B^b decreases towards I_A^b , the value of d_b decreases but d_B increases with the same amount and then $2d_b + 2d_B$ becomes constant. In the other hand, if $I_B^b = I_B^{b*} - \delta l$, all $I_B^f \geq I_B^{b*}$ are possible because I_A^f will

belong always to the interval given in the equation 2 (see figure 12).

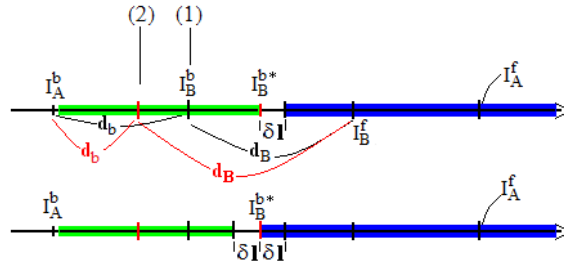


Figure 12: For a given I_A^f , possible values of I_B^b, I_B^f illustrated respectively in green and blue colors. If the value of I_B^b moves from the position (1) to the position (2), the value of $d_b + d_B$ is constant for a fixed value of I_B^f . If I_B^b is distant from I_B^{b*} by δl , the values of I_B^f may begin from I_B^{b*} .

It is necessary to have all combinations (I_B^b, I_B^f) in order to classify correctly all q outline pixels. To do this, we will use the following results:

- if we decrease I_A^f by $2\delta l$, the value of I_B^{b*} is decreased by δl (see figure 13) and thus we get new possible values of (I_B^b, I_B^f) .

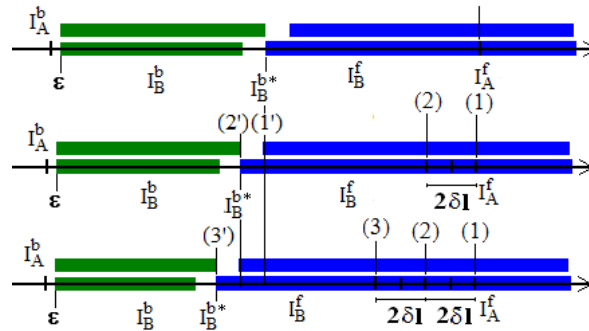


Figure 13: When the value of I_A^f is decreased by $2\delta l$, and translated from the position (1) to (2), the value of I_B^{b*} is decreased by δl and translated from (1') to (2'). Possible values of (I_B^b, I_B^f) are illustrated respectively by the green and blue colors. The same remark is valid when I_A^f is decreased again by $2\delta l$ from (2) to (3).

- if we increase I_A^b by $2\delta l$, the value of I_B^{b*} is increased by δl (see figure 14)

and thus we get new possible values of (I_B^b, I_B^f) .

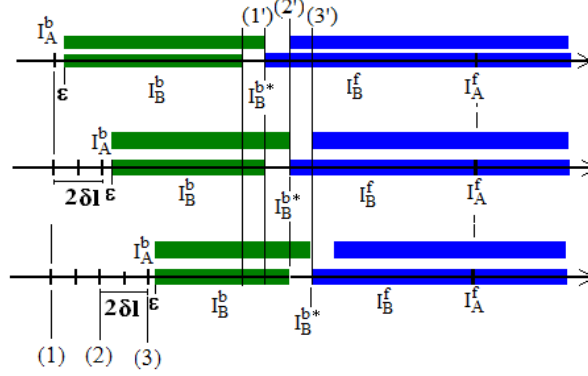


Figure 14: When the value of I_A^b is increased by $2\delta l$, and translated from the position (1) to (2), the value of I_B^{b*} is increased by δl and translated from (1') to (2'). Possible values of (I_B^b, I_B^f) are illustrated respectively by the green and blue colors. The same remark is valid when I_A^b is increased again by $2\delta l$ from (2) to (3).

Using these three results, we can get all combinations of (I_B^b, I_B^f) performing the following steps:

- (1)- Set $(I_A^b = 0)$ and $(I_A^f = 2\delta l)$, this implies that $I_B^{b*} = \delta l$.
- (2)- We increase the value of I_A^f with a step of $2\delta l$, this implies that I_B^{b*} increases with δl .
- (3)- We repeat the step (2) until that I_A^f reaches the high value of intensity 224, then I_B^{b*} reaches the value 112. I_A^f can't reach the value 255 because we can't have in this case $I_B^f > I_A^f$.
- (4)- The rest of I_B^b values are obtained by moving I_A^b and I_A^f .

If we take $\delta l = 16$, the set of (I_A^b, I_A^f) are :
 $(0, 32), (0, 64), (0, 96), (0, 128), (0, 160), (0, 192), (0, 224),$
 $(64, 192), (64, 224), (96, 224), (128, 224), (160, 224),$
 $(192, 224), (208, 240)$ which correspond to the following values of I_B^b :
 16, 32, 48, 64, 80, 96, 112, 128, 144, 160, 176, 192, 208, 224 (see figure 15).

What we propose in this paper is the use of artificial patterns $P_{1,i}$ instead of real images. The key idea is to generate the image A so as the background is set to zero (I_A^b) and the foreground is a shape having intensity I_A^f and representing the four main directions of the contours ($d_i, i = 0, 3$). This allows any q of $N(q)$ so as $I_B^f > I_B^b = (I_A^f - I_A^b)/2$ to be classified correctly (see figure 16). The

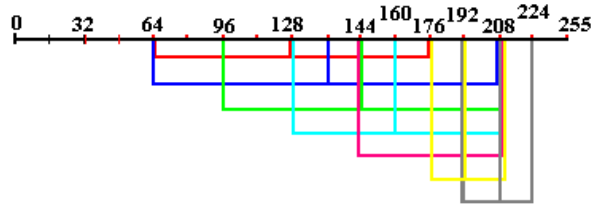


Figure 15: Used values of I_A^b, I_A^f for obtaining all I_B^b, I_B^f values

pattern I_A^f , identical to A but in addition contour pixels are marked.



Figure 16: Sample of used pair of patterns (A, A') where four directions are considered

We can now give the following result based on the previous reasoning:

Let (A, A') be an artificial pattern having I_A^b and I_A^f as intensities of the background and foreground. Let $N(q)$ be the neighborhood of the query pixel q so as I_B^b, I_B^f intensities of the two regions of $N(q)$ so as $(I_B^f > I_B^b)$ and $d_b = (I_B^b - I_A^b) > 0$. The pixel q will be classified correctly if $2d_b + 2d_B > I_A^f > 2d_b$.

The set of generated pairs of patterns $P_{1,i}$ as illustrated by figure 17.



Figure 17: The set of patterns $P_{1,i}$ in case of $d_b > 0$

Case 2

Our goal is to have the located outline pixels verifying: $d_b < 0$ and $d_A \in [2d_b + 2d_B, 2d_b]$.

Following the same reasoning as case 1, we get the following result:

Let (A, A') be an artificial pattern having I_A^b, I_A^f as intensities of the background and foreground. Let $N(q)$ be the neighborhood of the query pixel q so as I_B^b, I_B^f intensities of the two regions of $N(q)$ verifying $(I_B^f < I_B^b)$ and $d_b < 0$. The pixel q will be classified correctly if $2d_b + 2d_B < I_A^f < 2d_b$.

If we take $\delta l = 16$, the set values of (I_A^b, I_A^f) are: $(255, 224), (255, 192), (255, 160), (255, 128), (255, 96), (255, 64), (255, 32)$ giving the values of I_B^b equal to 240, 224, 208, 192, 176, 160, 144. The value 0 for I_A^f is excluded because this implies that $I_B^b = 128$ and then we can't have $I_B^f < I_A^f$.

To obtain other combinations, it is sufficient to take the following values for (I_A^b, I_A^f) :

$(224, 32), (192, 32), (160, 32), (128, 32), (96, 32), (64, 32), (48, 16)$ which correspond to the following values of I_B^b : 128, 112, 96, 80, 64, 48, 32.

The set of pairs of patterns $P_{2,i}$ as illustrated by figure 18.



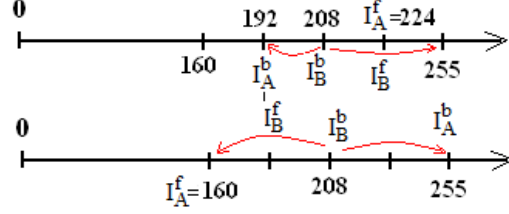
Figure 18: The set of patterns $P_{2,i}$ in case of $d_b < 0$

4.1 Duality of the two sets of artificial patterns

The two sets of artificial patterns proposed for contour detection ($P_{1,i}$ for the case $d_b > 0$ and $P_{2,i}$ for the case $d_b < 0$) perform the same task, the unique difference is the position of the computed contour which is outside of the shape for the first one and inside the shape for second one.

This duality is due to the fact that each case may be considered as the other case interchanging the role of the considered regions: the darkest region is considered as background and the clearest one as shape for the set of patterns and vice versa.

Figure 19 illustrates this duality for example between $P_{1,13}$ and $P_{2,3}$. For the pattern $P_{1,13}$, the possible values of I_B^f are from 208 to 255 and for I_B^b are from 208 to 192. Concerning the pattern $P_{2,3}$, the possible values of I_B^f are from 208 to 255 and for I_B^b are from 208 to 160. The second is then equivalent to the first one if we interchange between I_B^b and I_B^f .

Figure 19: Example of the duality between patterns $P_{1,i}$ and $P_{2,j}$

This relation is verified for the following pairs of patterns:

$$\begin{aligned}
 &(P_{1,1}, P_{2,1}), (P_{1,2}, P_{2,14}), (P_{1,3}, P_{2,13}), \\
 &(P_{1,4}, P_{2,12}), (P_{1,5}, P_{2,11}), (P_{1,6}, P_{2,10}), \\
 &(P_{1,7}, P_{2,9}), (P_{1,8}, P_{2,8}), (P_{1,9}, P_{2,7}), \\
 &(P_{1,10}, P_{2,6}), (P_{1,11}, P_{2,5}), (P_{1,12}, P_{2,4}), \\
 &(P_{1,13}, P_{2,3}), (P_{1,14}, P_{2,2}).
 \end{aligned}$$

4.2 Obtaining of most significant outline

When we visualize the located contour using two successive patterns $P_{1,i}$ and $P_{1,i+1}$ we find that the outline is either growing or shrinking. This motion of the outline is explained by the illustration in Figure 20. If we assume that outline are located for the pattern $P_{1,i}$ with $(I_{A,i}^b, I_{A,i}^f)$, then all contour pixels which verify $I_B^f > I_{B,i}^b$ will be located where $I_{B,i}^b = (I_{A,i}^b + I_{A,i}^f)/2$.

If the pattern $P_{1,i+1}$ is used, then $(I_{A,i+1}^b, I_{A,i+1}^f)$ replaces $(I_{A,i}^b, I_{A,i}^f)$ and $I_{B,i+1}^b$ instead of $I_{B,i}^b$ (see figures 20, 21).

For the second pattern $P_{1,i+1}$, all pixels verifying $I_B^f > I_{B,i+1}^b$ ($I_{B,i}^b < I_{B,i+1}^b$) will be located. Consequently, the pixels for which the value of I_B^f is between $I_{B,i+1}^b$ and $I_{B,i}^b$ will not appear in the new located outlines. These pixels correspond to low variation of intensity and are considered as high frequency information. Figure 21 illustrates an example where the green and blue colored contour (rightmost region in the segmentation) are located using $P_{1,i}$ pattern. However, the green outline does not appear when the pattern $P_{1,i+1}$ is used. Consequently, only the red and blue contour will be located.

The result of application of all patterns to the query image produces a set of outlines that are moving showing the propagation of high frequency outlines. We will associate a level of outlines the number of times where it appear applying a successive patterns $P_{1,i}$. For example, if we apply two successive patterns

P_i^1 and P_{i+1}^1 , outlines that appears only with $P_{1,i}$ are of level 1. Those which appear with both $P_{1,i}$ and $P_{1,i+1}$ are of level 2 and so on.

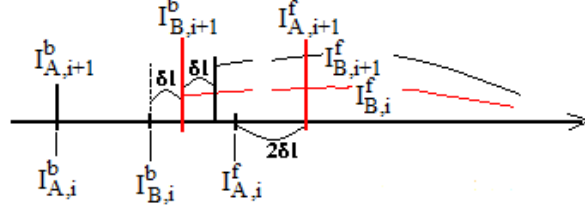


Figure 20: Evolution of the contour using successive patterns $P_{1,i}$ and $P_{1,i+1}$, here we took $I_{A,i}^b = I_{A,i+1}^b$

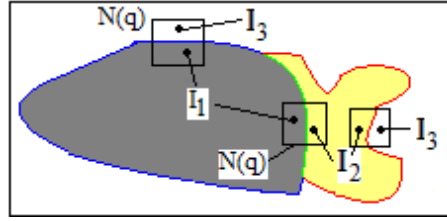


Figure 21: Example of the evolution of the contour: First the use of the pattern $P_{1,i}$ allows locating the outline in blue and green color because the intensities I_1, I_2 of $N(q)$ with (grey, White) colors and I_1, I_3 of $N(q)$ with (grey, yellow) colors verify the equation 2 where the $N(p)$ is taken from the defined $P_{1,i}$. The outline in red color is located only by the next pattern $P_{1,i+1}$ because the intensities I_2, I_3 of $N(q)$ with (yellow, white) color verify the equation 2 where the $N(p)$ is taken from the defined $P_{1,i+1}$.

In order to decrease the interval of recovering $[I_{B,i}^b, I_{B,i+1}^b]$, we will use $\delta l = 8$ instead of $\delta l = 16$. This allows to obtain more levels of contours. In this case, the number of patterns $P_{1,i}$ is 28 instead of 14 and the values of I_A^b, I_A^f become:

(0, 16), (0, 32), (0, 48), (0, 64), (0, 80), (0, 96), (0, 112),
 (0, 128), (0, 144), (0, 160), (0, 176), (0, 192), (0, 208), (0, 224),
 (0, 240), (64, 192), (64, 208), (64, 224), (64, 240), (96, 224), (96, 240),
 (128, 224), (128, 240), (160, 224), (160, 240), (192, 224),
 (192, 240), (208, 240).

The corresponding values of I_B^b are therefore:
 8, 16, 24, 32, 40, 48, 56, 64, 72, 80, 88, 96, 104, 112, 120, 128,
 136, 144, 152, 160, 168, 176, 184, 192, 200, 208, 216, 224.

5 Algorithm, Complexity and Details of the Implementation

The proposed method uses the 14 artificial patterns represented by pairs of images illustrated by figure 17. For a query image B of size $(N \times M)$, and for a size of the neighbors $N(q)$ equals to 3, each $N(q)$ associated to a pixel q , similarity measures $S(q, p)$ is computed for all $N(p)$ of the image A .

Let $(N' \times M')$ be the size of the image A . As $S(q, p)$ is computed $N'M'$ times for each q , the number of times of the computation of $S(q, p)$ for all pixels q is equal to $(N \times M \times N' \times M')$. The number of operations required for the computation of the similarity measure is equal to: $(m \times m)$ subtractions, $(m \times m)$ multiplications, and $(m \times m) - 1$ additions, assuming that $m \times m$ is the size of $N(q)$ (see equation 1).

Then for each pattern, to compute the pixels contours we need to perform: $(N \times M \times N' \times M')(3m \times m)$ arithmetic operations.

To reduce this complexity, we improved the computation of the similarity measure which instead to concern all the image A , we used only some neighbors $N(p)$ representing all the information of the image. Indeed, there is many time computation without any profit for the computation of $S(q, p)$ such as when $N(p)$ concern only the background or the foreground of A (see figure 22). To avoid this loss of time, we considered only all possibilities of $N(p)$ appertaining to the border of the shape inside A and to the background or the foreground.

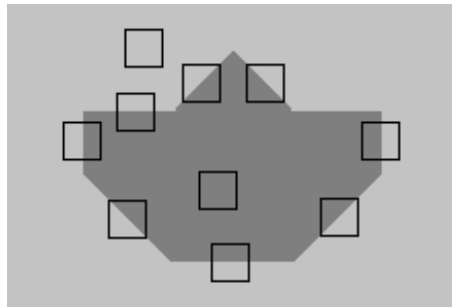


Figure 22: The considered $N(p)$ in the training image A

There are 8 considered Neighbors $N(p)$ considered as illustrated by figure 22. For each one containing a border, four configurations are considered giving all possibilities of the border in $N(p)$ as illustrated by figure 23.

With this new improvement, the number of used neighbors $N(p)$ in A is then equal to $24 + 2$ (2 for the foreground and background).

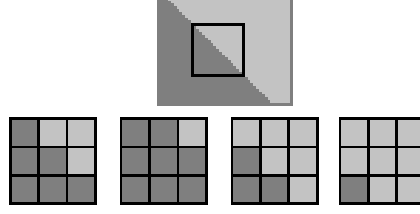


Figure 23: Example of considered $N(p)$ and the different configurations taken into account for such neighbor

The number of arithmetic operations using the 14 patterns is then equal to: $(14 \times N \times M \times 26 \times (3m \times m))$ giving a complexity of $O(n^2)$.

If we consider for example, one image of BSD500 dataset having (481×321) rows and columns, the number of operations is equal to: $(14 \times 481 \times 321 \times 26 \times 27) = 1517453028$ operations.

Most microprocessors today can do 4 FLOPs per clock cycle. Therefore, a single-core 2.5 GHz processor has a theoretical performance of 10 billion FLOPS = 10 GFLOPS, this gives as computation time equal to 0,151sec.

The Algorithm

Begin

- (A, A') is the pair of artificial training pattern

- B is the query image

- B' is the computed image, identical to B , in addition contour pixels will be marked

-The 26 reference $N(p)$ in A are used instead of all $N(p)$ of A

For each q from B

Do For each reference $N(p)$ of A

Do Compute the similarity measure $S(q, p)$

EndFor

Select p^* so as $S(q, p^*)$ is minimal

If (p^* in A' is a contour pixel)

Then q is set in B' as contour pixel

Else q is set in B' as non contour pixel

EndFor

End.

6 Results

The first part of this section is devoted to the parameter setting and to results obtained using images of hand-drawn contours as training images. In particular we discuss the limitations of this approach. We show how the detected contour varies through the image depending on the specific variation of luminosity chosen, resulting in a contour "level". The problem of the choice of the suitable patterns in order to find the expected contour has been studied in 4.2 and the result of computation of contours of different levels is presented. We applied our method to the problem of detecting people in video sequences (a focus of CAVIAR data set). We show that the detection is easily achieved due to the quality of contours acquired by our method.

We present in the next, a study related to the invariance of located contours to scale change and rotation. Finally, we present a qualitative and quantitative evaluation of our method on different data sets of real images: Berkeley Segmentation Data Set (*BSDS500*) (3), Weizmann Horses (7). The BSD 500 consists of 500 natural images, with hand drawn contours by five different subjects. Weizmann Horses data set consists of 328 images of horses manually segmented. Only the outlines of horses are drawn. The obtained results are compared with the state of the art methods. Finally, we studied the invariance of the proposed method to scale change and rotation.

6.1 New benchmarks for BSD 500 dataset

The definition of contour such is given by is:

Since human judgment is the only possible criterion that can be used in order to say if a given visual feature is a contour or not, we operationally define contours in a given image as the set of lines that human observers would consent on to be the contours in that image (one could give a similar operational definition of other concepts used in the image processing and visual pattern recognition literature, such as face). On the light of this, research in contour detection aims at understanding and modeling mathematically the features which people (consciously or unconsciously) use to recognize such line sets (such as contrast, good continuation, and closure).

6.2 Parameter settings

There are three parameters whose values are justified: the size of neighborhoods $N(p)$ and $N(q)$, the number of directions of contours in training images (artificial patterns) and the value of δl .

- Size of neighborhoods $N(p)$ and $N(q)$: In 3.2, we have seen that the optimal match p of a query pixel q will be obtained so as the directions of contour pixels in both $N(p)$ and $N(q)$ are the same.

When this size of $N(p)$ and $N(q)$ is equal to 3, more contours pixels will be located because the three aligned contour pixels will more numerous than with size more greater (5 or 7). Figures 24, 25, 26 illustrate the located contours using the pattern P_5 for the value of size is equal to 3, 5 and 7. We can see that with $size = 3$, contour pixels encompass with more accuracy the regions and are more numerous than with other sizes. When the size is equal to 5 or 7, in the query image, there are less possibilities to have aligned contour pixels having the same direction such as $N(p)$. Indeed, despite the quality of the contours are the same, some contours pixels will be not located in addition of the time of computation that will increase considerably.



Figure 24: Located contours using the pattern P_5 for sizes of neighborhood $N(p)$ equal to 3

- Number of directions: We considered in the different illustrative figures of the paper four main directions. With size of the neighborhood $N(q)$ equal to 3, all directions are represented with the four considered directions and then it



Figure 25: Located contours using the pattern P_5 for sizes of neighborhood $N(p)$ equal to 5

is sufficient to locate any contour orientation. Figure 27 illustrates a sample of shape whose boundaries have other directions than the four considered, but all contour pixels are located using size of the neighborhood $N(q)$ equals to 3 which looks with uniform connexity (a 8-connected); while with a neighborhood size equals to 5 the contour are with two different connexities (pixels are 4 and 8-connected).

- Value of δl : The set of artificial patterns are based on the value of δl : the 14 patterns will be used if this value of δl is equal to 16 and 28 patterns will be used if value is equal to 8 .

The values of these parameters are known and the computed contours does not depend from any other parameter and are unique for each image.

6.3 Using hand-drawn contours as training images

To detect the outline of a query image, we require a pair of training images (A, A') of a scene where A' is identical to A , in addition it contains hand-drawn contours.



Figure 26: Located contours using the pattern P_5 for sizes of neighborhood $N(p)$ equal to 7

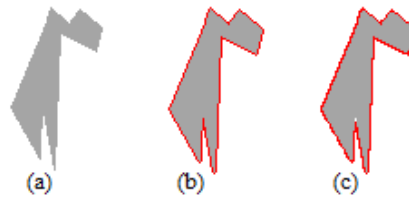


Figure 27: (a) Initial image, (b) Located contours using the size of the neighborhood $N(q)$ equals to 3, (c) Located contours using the size of the neighborhood $N(q)$ equals to 5

Figure 28 illustrates images A, A' from the CAVIAR data set (where hand-drawn outline shapes are highlighted with red color). The automatically located contours for some images of the same video are illustrated by the same figure 28. It can be seen that in the query images some outlines are located but many others aren't located. This is because the neighboring to considered pixels do not verify the required constraints (see annex 9).



Figure 28: From top to bottom, left to right: Initial image A , The synthesized image A' , Located contours for a new frame B , Located contours for another frame B

Despite this limitation, hand drawn contours as reference may be used e.g. for the tracking of a moving object. In this case, it is sufficient to locate the strong foreground outline of the required object. Figure 29 illustrates some frames of CAVIAR video where a human is detected in each frame. The hand drawn image used as training image is taken from the same video set but not the same image.

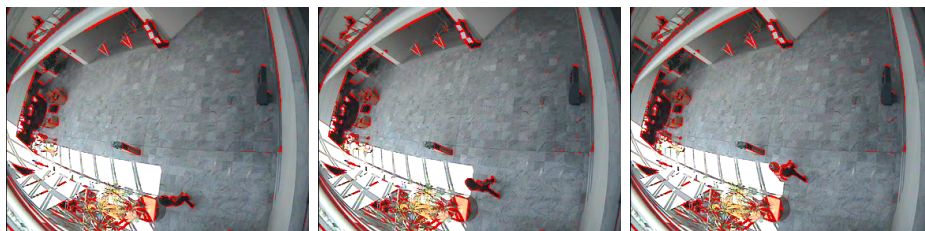


Figure 29: Contours located for four frames of CAVIAR video

6.4 Using pairs of artificial patterns as training images

Each one of the 14 pairs artificial patterns (A, A') enables us to detect a specific level of contour depending on the intensities of the neighboring regions to the border. Figure 30 illustrates contours located on the same frame of CAVIAR

video using some patterns of the set of 14 patterns. We can see that the outline is moving in image as explained in subsection 4.2 from the darkest region (applying the pattern $P_{1,1}$) to the clearest one (applying the pattern $P_{1,14}$).

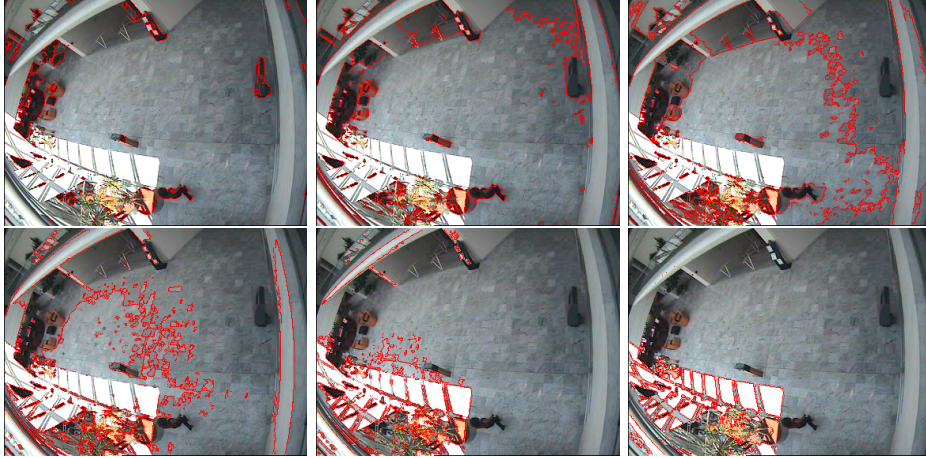


Figure 30: Contours computed using the patterns $P_{1,3}$, $P_{1,5}$, $P_{1,7}$, $P_{1,9}$, $P_{1,11}$, $P_{1,14}$

The application of one level over a set of frames from the CAVIAR video produced the results shown by figure 31. In this case the suitable pair of patterns have been chosen in order to locate the moving human. Indeed, if another pair of patterns is applied, the human outline will be (or partially) not located depending on how well it is represented in the training image.

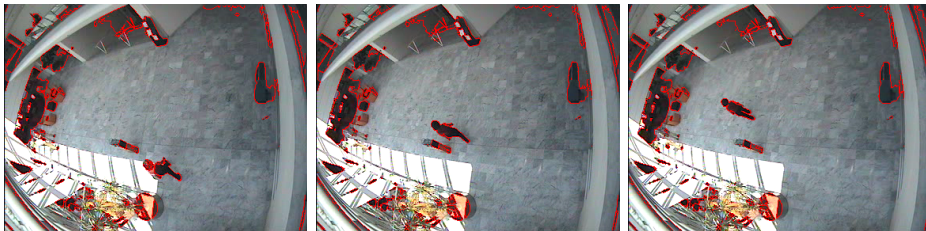


Figure 31: Contours located using the pattern $P_{1,4}$ for a first, a second frame, and a third frame of the CAVIAR dataset

6.5 Contour detection at different levels of resolution

The proposed method as described in the previous section allows to detect contours in image specifying the required level. This level is related to the intensity variation between pixels at the sides of the outline contour. The level l is associated to the contour which is located by successive l patterns: $P_j^1, P_{j+1}^1, \dots, P_{j+l-1}^1$. Then the position of the correspondent value I_B^f for such contour is located by the recovering of the intervals $]I_{B,j+k}^b, 255]$, $k = 0, l - 1$ as seen in subsection 4.2.

Figure 32 shows an example of located contours on image of BSD dataset using the set of 14 pairs of artificial patterns. We can see the low frequency outlines which correspond to the value of $l = 4$ and the high frequency outlines which correspond value of $l = 1$. The color black is associated to contours of level 4 and colors red, green and blue are used to distinguish the new contours detected for the considered levels 3, 2 and 1. The use of the set of 28 instead of 14 pairs of patterns for the same image produces contours at higher resolution for the same level. In summary, more the level is greater, more outline contours are found and thus contours corresponding to high difference of intensity between regions will remain in the computed image.

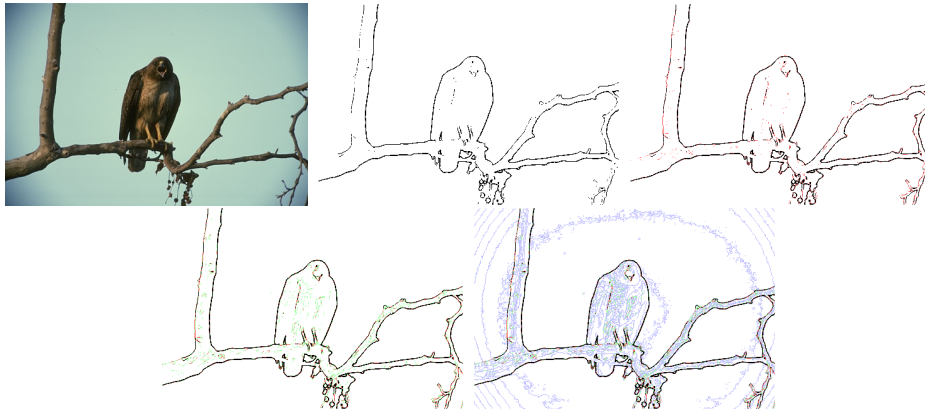


Figure 32: Original image, Contours of level 4, 3, 2 using the 14 patterns

6.6 Affine transformation Invariance

We studied the invariance of our method to affine transformation such as rotation, scale change. We compared the rotated contours computed for initial images and the contours located after image rotation. We considered for this all contour images obtained using the set of 14 pairs of patterns. We measured

the ratio of contour pixels that haven't been located after image rotation and computed the average of this ratio for different images with different angles of rotation (lena, BSD500 data set). This ratio is around 0.02 for any rotation angle. Figure 33 illustrates images obtained for "lena" image and the computed contours shown with red color.

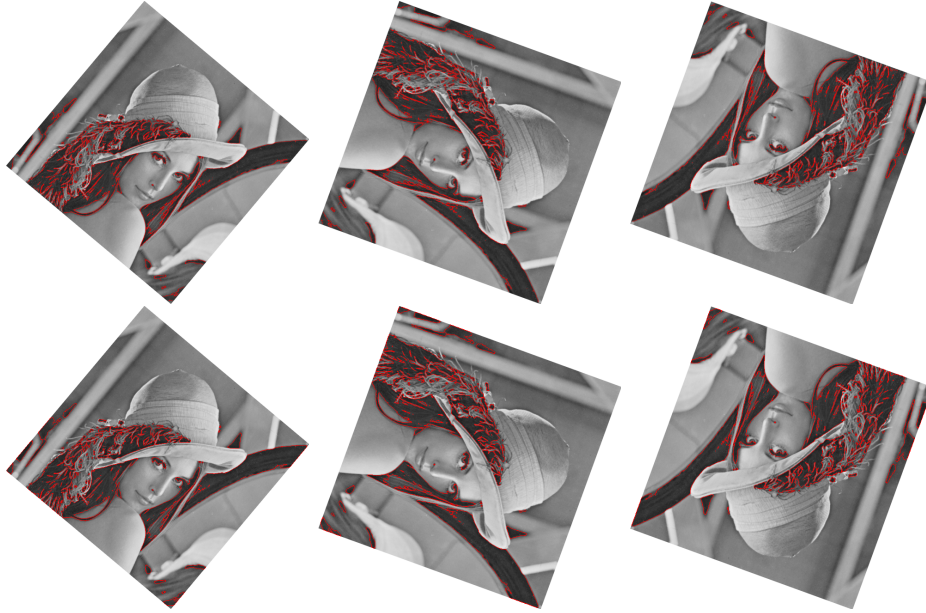


Figure 33: From top to bottom, left to right: Rotated images of contours located using the pattern P_4 and the angle 40° , 110° , 200° . Contours of rotated images located using the pattern P_4 and the angle 40° , 110° , 200°

For scaling invariance study, we applied contour detection after scaling images to 90%, 80%, 70%, 50%, 40%, 25%, 12.5% of its original size (see figures 34, 35, 36).

The scaling has been done using "paint" software and we can see that under 50 the quality of image is degraded. We measured the ratio of contour pixels that haven't been located after image scaling related to the scaled contours of original image. Experiments have been conducted on BSD500 data set and the average of this ratio computed from all images obtained using the 14 patterns on BSD dataset images gave: 0.04, 0.05, 0.09, 0.17, 0.26, 0.33 corresponding to scaled original image to 80%, 70%, 60%, 50%, 25%, 12%.

Despite that the used images are scaled with software, we can see that above 50%, our method is invariant to scaling. Below of 50%, images are very

degraded and thus locating contours will produce a missing of original pixels contours due to missing of information.



Figure 34: Original image, Scaled image to 70%, Scaled image to 40%, Scaled image to 25%



Figure 35: Computed contours using the pattern P_5 for the scaled images



Figure 36: From left to right: Computed contours using the pattern P_5 , Scaled contours of the original image to 70%, 40%, 25%

7 Evaluation and Discussion

Many evaluation measures have been proposed for boundary quality and for all them there is a necessity to have the ground-truth data represented by the correct pixels contours drawn by hand. Estrada et al (20) considered this measure as related to the quality of the segmentation of the image induced by the computed contour where the best boundary neatly separates two visually distinct regions of the image. The error measure based on the average distance between boundary pixels from two contours is used. The inconvenience of this measure is that is necessary to match all computed outlines and all the reference ones.

Other measure proposed by Martin et al (35; 3) considers the ratios - precision, recall - computed using the numbers of pixels found in the automatic contours vs the correct (hand-drawn) ones. This measure may do a good job of estimating the quality of found contours only if two conditions are verified otherwise it gives a false estimation of the quality. The first condition is that both the computed and reference contours must be of the same resolution which means that if the method locates only a specific resolution of contours (levels in our scheme), the used hand drawn contour must also have the contours at that resolution. The second condition is that the task of reference contours drawing must be done with high accuracy and all possible contours must be located for the ground truth data.

As example, we cite the data set BSD500 (3) where for each image, five hand

drawn contours are available. Our opinion is that such reference images must be used as benchmark for segmentation algorithms rather than contour detection algorithms because only shapes are segmented and some true contours are not located even if they separate two visually distinct regions. In our experiments, we built our reference images for the BSD 500 dataset.

7.1 Visual estimating of the quality of contour detection: some samples

We give in this subsection some results obtained by our method for visual comparison with the results obtained by the algorithms of Berkeley (3) and Canny (9) performed on BSD500 data set.

The reader can easily identify on the illustrated results which is the best computed image of contours. The strong advantage of our method is that the computed contour pixels are located only when there is a transition between two regions. Depending of the resolution used (high, intermediated or low), the precision of located contours by our method is better than the precision of located by Berkeley (3) and Canny (9). Indeed, Canny's algorithm depends on the used thresholds and then when there are more pixels of contours, there will be consequently more and more false candidates. Concerning the method of Berkeley (3), many good candidates are missing and then is more suitable for image segmentation. Indeed, the making of BSD data set has been done by subjects satisfying this criterion. Only the outlines of objects are drawn. Consequently, this algorithm has outperformed all contours detection algorithms on this data set.

For example, seeing to figures 37, 38, the owl is clearly more recognizable from our contours than perceiving other results. On the canny result, there are many false candidates and the image of contours looks like a random dot stereogram. For Berkeley result, many contours are missing.



Figure 37: Image from BSD500 data set, Located contours by Arbelaez algorithm

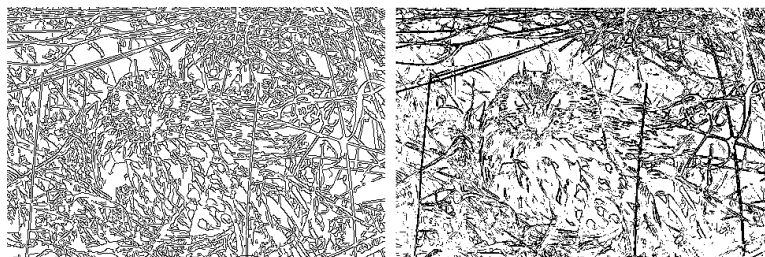


Figure 38: Located contours by Canny algorithm with high threshold equals to 300, Located contours by our method with intermediate resolution

The canny method fails to detect texture for some images of BSD 500. In figures 39-40, our method localizes the texture on the center of the image with high precision, however Canny fails completely. The same case is repeated for another image as illustrated by figures 39 to 42 where Canny encounters a problem for locating the texture at low left of the image. For the two images, Berkeley does not locate all textures.



Figure 39: Image from BSD500 data set, Located contours by Arbelaez algorithm

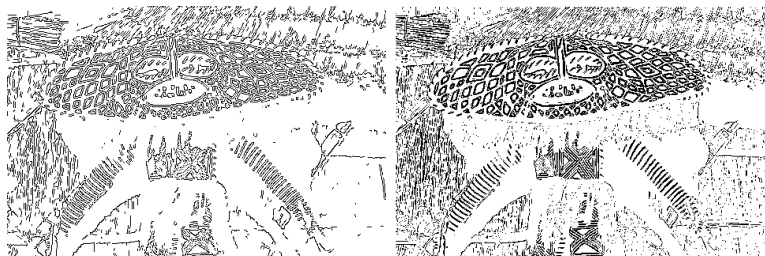


Figure 40: Located contours by Canny algorithm with high threshold equals to 300, Located contours by our method with intermediate resolution



Figure 41: Image from BSD500 data set, Located contours by Arbelaez algorithm

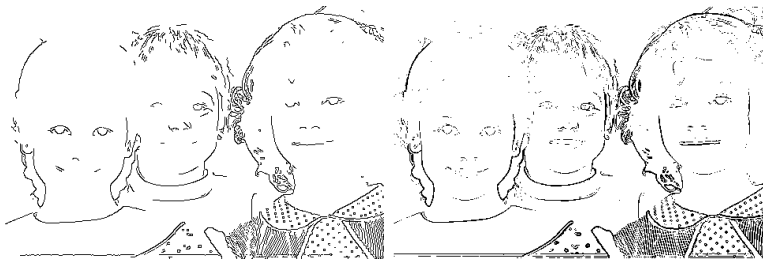


Figure 42: Located contours by Canny algorithm with high threshold equals to 300, Located contours by our method with intermediate resolution

7.2 Evaluating contour detection quality on BSD500 data set

We compared our results to those obtained by Canny's and Berkeley's methods. Canny is selected because it uses only the low level feature (intensity), and Berkeley is selected because it uses some mid-level features (patch descriptor, texture, histogram). Similar results to those of P. Arbelaez *et al.* (3) are obtained by some algorithms which have used mid-level and high level information in order to locate the outlines of objects such as (8; 17; 54) and (39) which is contour-based method starts from located contours, locates boundary and performs their grouping. The results of these methods are then have not been considered.

For the BSD500 data set, we computed the Precision and Recall and we obtained best results than those of gPb method of Arbelaez *et al.* (3) and Canny method (9).

The maximum of $F - measure = 2.Precision.Recall / (Precision + Recall)$ for our method is equal to 0.74 which is greater than Canny with 0.65 and Berkeley with 0.49. (3) (see figure 43). This superiority is due to two fac-

tors. The first one is that our method locates all pixels of contours such as do Canny, however, we outperform Canny which depends on the thresholds. If more contours are located, the precision decreases, with the increase of Recall. If less contours are located, Recall decreases and Precision increases. The second one is the used ground truth made by drawing all contours. This new data set cannot produce good results for the methods which located outlines than contours.

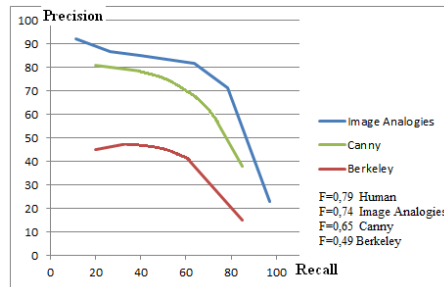


Figure 43: Recall and Precision of contour detection approaches on BSD500 dataset with respect to human ground-truth boundaries

7.3 Evaluating contour detection quality on Weizmann Horses data set

We repeated the same experiments for Weizmann Horses data set (7) and our results are compared to the results of Payet and Todorovic (39) and gPb method (32) (see figure 44). We note that for the ground truth data only the horses are located. Consequently, methods which locate outlines rather than contours are favourites to obtain best scores of (Recall, Precision). The obtained results will be better if all contours are located in the ground truth data.

Figure 45 illustrates a sample of images from this data set and the reference contours are made by locating only horses from background. Our computed contours are precise. However, as all pixels are counted in the evaluation of the quality measure, most of the values obtained (Recall, Precision) for all images are under to those obtained by SLEDGE and gPb methods. This low performance is due to numerous contours located of the background in addition to internal ones of the horse (see figures 45, 46).

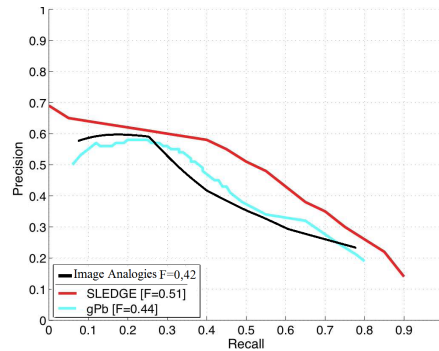


Figure 44: Recall and Precision scores obtained for Weizmann data set

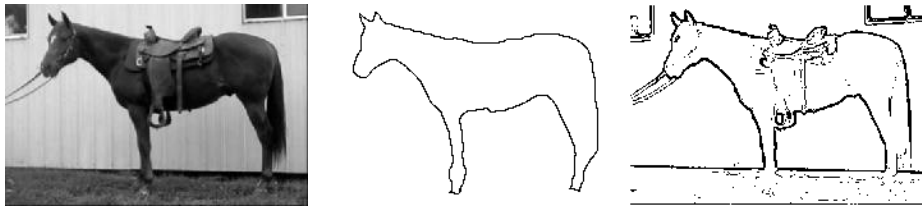


Figure 45: First image from Weizmann Horses data set, Ground truth data, Our computed contours

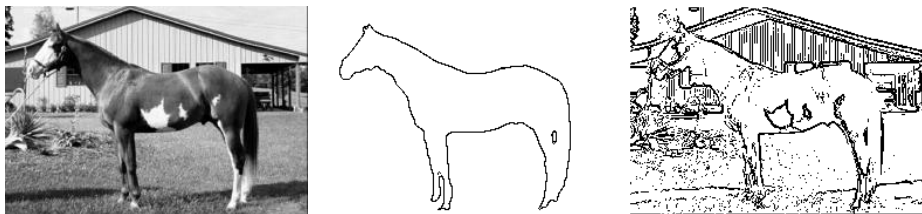


Figure 46: Second image from Weizmann Horses data set, Ground truth data, Our computed contours

7.4 Discussion

The resolution level of contours must be defined in order to make suitable benchmarks for comparison of contour algorithms. In the step of reference image making, the human completes some parts of outline shapes that are not neatly visible because he uses his/her prior knowledge about the shape geometry and locates the perceived contours without specifying their levels. That is, it is a cognitive process based around shape extraction, not contours *per se*.

In this work the level of contour (as stated above) is related to the difference of intensity between neighboring regions. In our comparison, we used reference images where contours are hand drawn by human subjects without specifying the level of contours. In this case, we computed the contours for level 1, 2, 3 and 4 using 14 artificial patterns for the computation of Recall and Precision.

Our method cannot localize contours when the human himself cannot (note we are not talking about inferring the presence of a shape, but an actual contour). This occurs when the part of shape and the background have the same color or intensity. Such cases have decreased the performance of our method. Even if all these contours may be localized at the level 1, they cannot be exploited due to the high number of contour pixels found for this level.

8 Conclusion

We proposed in this paper a new method for contour detection based on image analogies. In the first part, we studied the possibility to use of hand-drawn contours as reference images for the detection of new contour pixels by analogy in the query image. We found that only pixels that have the same conditions as those of the reference image may be located which is perhaps to be expected in such a data driven technique. This implies that numerous reference images are needed to locate all possible new contour pixels which implies in the hard and time-consuming task of hand drawing reference contours, and thus increasing of the algorithm complexity.

Instead to apply directly image analogies, we investigated in this work, how can we avoid this constraint in order to guaranty that all contour pixels will be located for any query image. Fourteen derived patterns are sufficient to be used as training images (instead of real images alone) to locate contour location at different scales independently of the light conditions present in the real images.

To avoid this constraint and to locate all contour pixels whatever the image query happens to be, we proposed a set of 14 artificial pairs of patterns as reference images of low size and containing the required information to locate contours of different levels of resolution where levels are related to the difference of intensity between neighboring regions.

The proposed method has been applied to different types of images: the “natural” BSD dataset, Horses of Weizmann data set. Compared to the reference images, our method demonstrates a very good recall, precision and finds all visible contours of gray level images.

8.1 Further work

We note that, as the technique is based only on intensity attributes, some contours separating colored regions that are visible are not located due to the close values of region intensity. Because our approach uses only intensity, we are confident that including color attributes in the similarity measure will increase the performance of the method and decrease the failure modes.

Also, an interesting work will be the exploitation of the set of contours computed with the artificial patterns for image segmentation. Indeed, seeing the computed contours from one pattern to another, we can notice that there is a slow motion of contours around the region boundaries.

it will be interesting the modeling what human do in similar way.

9 Appendix: Constraints required for images training

We study, given the proposed similarity measure, what are the required constraints in the training images in order to locate all and only contour pixels.

We consider the general case where intensity in image is not uniform around the boundary and we will take into account complicating factors such as gradually changing shading or texture.

We distinguish the two cases where the pixel q in the query image B is a contour pixel or not .

case (1): q isn't a contour pixel

Under this hypothesis, we study if the selected pixel p^* could be a contour pixel?

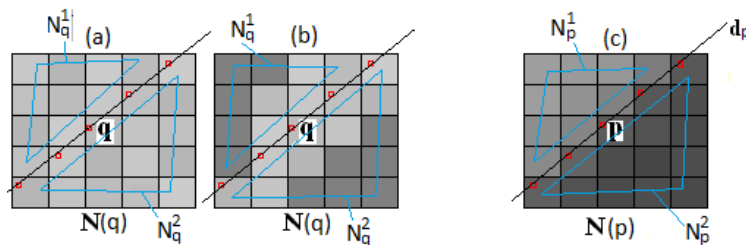


Figure 47: (a) q isn't a contour pixel and $N(q)$ doesn't contain contour pixels (b) q isn't a contour pixel and $N(q)$ contains some contour pixels, (c) p is a contour pixel

Let d_p be the line of contour pixels in $N(p)$ defining two regions N_p^1, N_p^2 . $N(q)$ is also divided into two regions N_q^1, N_q^2 following the same direction of the line d_p (see figure 47).

The similarity measure $S(q, p)$ between $N(q)$ and $N(p)$ is then given by the equation 5:

$$S(q, p) = \sum_i \sum_j (N_q^1(i, j) - N_p^1(i, j))^2 + \sum_i \sum_j (N_q^2(i, j) - N_p^2(i, j))^2 \quad (5)$$

Where $N_p^1(i, j), N_p^2(i, j)$ (respectively $N_q^1(i, j), N_q^2(i, j)$) are the intensities of pixels (i, j) of regions N_p^1, N_p^2 (resp. N_q^1, N_q^2).

As the pixel p is a boundary pixel, there is a difference of intensity between the pixels of regions N_p^1, N_p^2 . It is sufficient to find in A the neighbor $N(p)$, such as p is not a contour pixel, which produces a similarity measure less than $S(q, p)$ obtained with $N(p)$ having p as contour pixel. Indeed, the value of $S(q, p)$ is greater than $S^1(q, p)$ obtained when $N(p)$ is taken entirely from a region like N_p^1 ($N_p^2 = N_p^1$) and either $N_q^2(i, j) < N_p^1(i, j) < N_p^2(i, j)$ or $N_q^2(i, j) > N_p^1(i, j) > N_p^2(i, j)$. Also, the value of $S(q, p)$ is greater than $S^2(q, p)$ obtained when $N(p)$ is taken entirely from a region like N_p^2 ($N_p^1 = N_p^2$) and either $N_q^1(i, j) < N_p^2(i, j) < N_p^1(i, j)$ or $N_q^1(i, j) > N_p^2(i, j) > N_p^1(i, j)$.

Consequently, the q pixel of B can't be classified as a contour.

case (2): q is a contour pixel

In this case, we will study if the similarity measure $S(q, p)$ is minimal when the pixel p is a contour pixel. Otherwise, we must find the required conditions such that a contour pixel p will be selected as the best match for q .

As q is assumed as a contour pixel, let d_q the direction of the boundary in $N(q)$. $N(p)$ is assumed to have any structure and the direction d_p of its boundary may be different from the direction d_q of $N(q)$, the central pixel p could not be a contour pixel (see figure 48).

For each pixel q , the best match p^* is computed exploring all $N(p)$ in A and chosen so as the similarity measure $S(q, p^*)$ is minimal.

In order to determine the required conditions such that the computed best match p^* of q will be a contour pixel, we study the variation of $S(q, p)$ related to $N(p)$ structure and the intensities of pixels inside of $N(p)$ and $N(p)$. We note that the central pixel p may be or no an outline pixel.

Let:

- $S(q, p)$ be the value of the similarity measure such that $N(q), N(p)$ have the same structure: q, p are both contour pixels, and the directions of the

boundaries inside $N(q), N(p)$ are identical $d_q = d_p$.

- $S(q, p')$ be the values of the similarity measure such that $N(q), N(p')$ have different structures and p' may be or no a contour pixel.

$S(q, p), S(q, p')$ are given by the equations 6 and 7 where:

- $N_p^1(i, j), N_p^2(i, j), N_p^3(i, j), N_p^4(i, j), N_q^1(i, j), N_q^2(i, j), N_q^3(i, j), N_q^4(i, j)$ are pixels of regions $N_p^1, N_p^2, N_p^3, N_p^4, N_q^1, N_q^2, N_q^3, N_q^4$,

- $N_{p'}^1(i, j), N_{p'}^2(i, j), N_{p'}^3(i, j), N_{p'}^4(i, j)$ are pixels of regions $N_{p'}^1, N_{p'}^2, N_{p'}^3, N_{p'}^4$.

These regions are defined from the two assumed different orientations d_q and $d_{p'}$ of the boundaries in $N(q)$ and $N(p')$ (see figure 48):

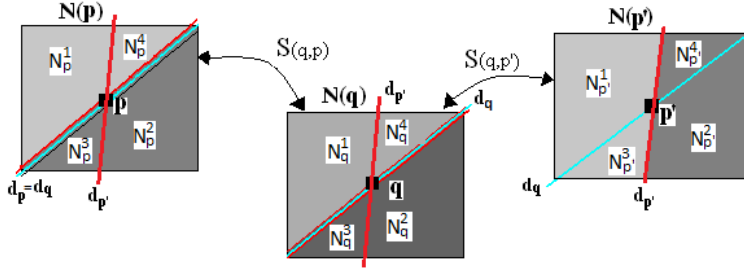


Figure 48: A same direction for the boundaries inside $N(q)$ and $N(p)$ and different directions for the boundaries inside $N(q)$ and $N(p')$, p' is a contour pixel

$$S(q, p) = \sum_i \sum_j (N_q^1(i, j) - N_p^1(i, j))^2 + (N_q^2(i, j) - N_p^2(i, j))^2 + (N_q^3(i, j) - N_p^3(i, j))^2 + (N_q^4(i, j) - N_p^4(i, j))^2 \quad (6)$$

$$S_m(q, p') = \sum_i \sum_j (N_q^1(i, j) - N_{p'}^1(i, j))^2 + (N_q^2(i, j) - N_{p'}^2(i, j))^2 + (N_q^3(i, j) - N_{p'}^3(i, j))^2 + (N_q^4(i, j) - N_{p'}^4(i, j))^2 \quad (7)$$

To compare between $S(q, p)$ and $S(q, p')$, we compute $\Delta S = S(q, p') - S(q, p)$ such that p and p' are assumed to be pixels of the same region which implies that $N_p^1 = N_{p'}^1, N_p^2 = N_{p'}^2$. We get:

$$\Delta S = \sum_i \sum_j (N_q^3(i, j) - N_{p'}^3(i, j))^2 + (N_q^4(i, j) - N_{p'}^4(i, j))^2 - (N_q^3(i, j) - N_p^3(i, j))^2 - (N_q^4(i, j) - N_p^4(i, j))^2 \quad (8)$$

The same equation is obtained in case where $N(p')$ has a different structure than $N(p)$ and p' isn't a contour pixel (see figures 49, 50).

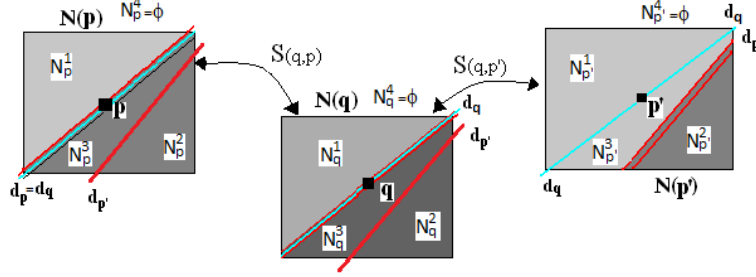


Figure 49: $N(p')$ having different structure than $N(q)$ and p' isn't a contour pixel

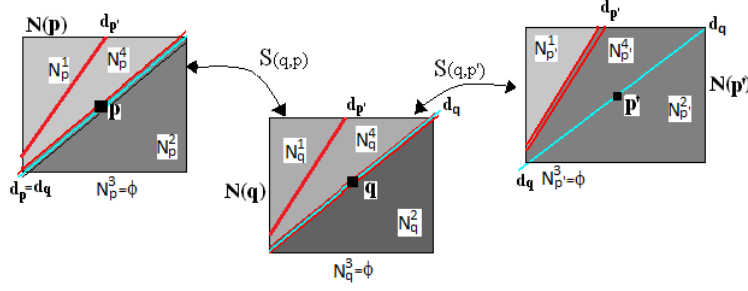


Figure 50: $N(p')$ having other different structure than $N(q)$ and p' isn't a contour pixel

The neighbor $N(p)$ having the same structure as $N(q)$ will be selected if the difference $\Delta S = S_m(q, p') - S(q, p)$ is positive.

Let I_A^b, I_A^f (resp. I_B^b, I_B^f) be the average of pixels intensities of the two regions of $N(p)$ (resp. $N(q)$). Otherwise, the average of intensities will concern all pixels of $N(p)$, $N(q)$ and will be noted I_A^b, I_B^b . Note here that the pixels of the same region in $N(p)$ and $N(q)$ are assumed have different values of intensities and then we are in complicating factors such as gradually changing shading or texture, but there is a boundary between them such that human can draw it.

We will use the following notations (see figure 48):

- $I_A^b, I_A^{lb}, I_A^{mb}$ be the average, minimal, maximal intensity of all $N_p^1(i, j), N_p^4(i, j), N_{p'}^1(i, j), N_{p'}^3(i, j)$ pixels,
- $I_A^f, I_A^{lf}, I_A^{mf}$ be the average, minimal, maximal intensity of all $N_p^2(i, j), N_p^3(i, j), N_p^{l2}(i, j), N_p^{l4}(i, j)$ pixels,

- $I_B^b, I_B^b, I_B^{''b}$ be the average, minimal, maximal intensity of all $N_q^1(i, j), N_q^4(i, j)$ pixels ,
- $I_B^f, I_B^f, I_B^{''f}$ be the average, minimal, maximal intensity of all $N_q^2(i, j), N_q^3(i, j)$ pixels.

Firstly, we assume that $I_A^b < I_B^b < I_B^f < I_A^f$ (see figure 51), the terms of the equation 8 can be written as follow:

$$\sum_i \sum_j (N_q^3(i, j) - N_{p'}^3(i, j))^2 > n_1 (I_B^f - I_A^{''b})^2 \quad (9)$$

$$\sum_i \sum_j (N_q^4(i, j) - N_{p'}^4(i, j))^2 > n_2 (I_B^{''b} - I_A^f)^2 \quad (10)$$

$$- \sum_i \sum_j (N_q^3(i, j) - N_p^3(i, j))^2 > -n_1 (I_B^f - I_A^{''f})^2 \quad (11)$$

$$- \sum_i \sum_j (N_q^4(i, j) - N_p^4(i, j))^2 > -n_2 (I_B^{''b} - I_A^b)^2 \quad (12)$$

where n_1 and n_2 are respectively the number of pixels of the regions $N_p^3, N_{p'}^3, N_q^3$ and $N_p^4, N_{p'}^4, N_q^4$ (see figure 48). The value of ΔS is then given by the equation 13.

$$\Delta S > n_1 (I_B^f - I_A^{''b})^2 + n_2 (I_B^{''b} - I_A^f)^2 - n_1 (I_B^f - I_A^{''f})^2 - n_2 (I_B^{''b} - I_A^b)^2 \quad (13)$$

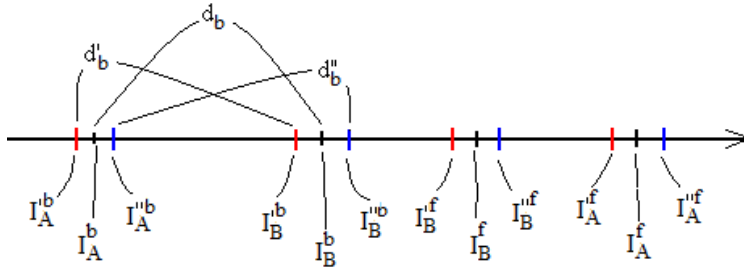


Figure 51: Example of possible values of $I_A^b, I_B^b, I_B^f, I_A^f$

We will note:

$$- d_A = I_A^f - I_A^b, d'_A = I_A^{''f} - I_A^b, d''_A = I_A^{''f} - I_A^{''b}$$

$$\begin{aligned}
& -d_B = I_B^f - I_B^b, d'_B = I_B^f - I_B^b, d''_B = I_B^{''f} - I_B^{''b}, \\
& -d_b = I_B^b - I_A^b, d'_b = I_B^b - I_A^b, d''_b = I_B^{''b} - I_A^{''b}, \\
& -\Delta I_B^f = I_B^{''f} - I_B^f, \Delta I_A^f = I_A^{''f} - I_A^f, -\Delta I_B^b = I_B^{''b} - I_B^b, \Delta I_A^b = I_A^{''b} - I_A^b
\end{aligned}$$

As:

$$\begin{aligned}
& n_1(I_B^f - I_A^{''b})^2 - n_1(I_B^f - I_A^{''f})^2 = n_1(I_B^f - I_A^{''b} + I_B^f - I_A^{''f})(I_B^f - I_A^{''b} - I_B^f + I_A^{''f}) \\
& = n_1(I_B^f - I_A^{''b} + I_B^f - I_A^{''f})(d''_A) \\
& \quad I_B^f - I_A^{''b} + I_B^f - I_A^{''f} = 2(I_B^f - I_B^b) + 2(I_B^b - I_A^b) + 2(I_A^b - I_A^{''b}) - (I_A^{''f} - I_A^{''b}) \\
& = 2d'_B + 2d'_b - 2 \Delta I_A^b - d''_A
\end{aligned}$$

and

$$\begin{aligned}
& n_2(I_B^{''b} - I_A^f)^2 - n_2(I_B^{''b} - I_A^b)^2 = n_2(I_B^{''b} - I_A^f + I_B^{''b} - I_A^b)(I_B^{''b} - I_A^f - I_B^{''b} + I_A^b) = \\
& n_2(I_B^{''b} - I_A^f + I_B^{''b} - I_A^b)(-I_A^f + I_A^b) = n_2(2d''_b - d'_A + 2 \Delta I_A^b)(-d'_A)
\end{aligned}$$

We obtain then; $\Delta S > n_1 d''_A (2d'_B + 2d'_b - 2 \Delta I_A^b - d''_A) - n_2 d'_A (d''_b + d'_b)$

We can consider that $d''_B = d'_B = d_B$, $d''_A = d'_A = d_A$, $d''_b = d'_b = d_b$ (see figure 51). We write then:

$$\Delta S > n_1 d_A (2d_B + 2d_b - d_A - 2 \Delta I_A^b) - n_2 d_A (2d_b - d_A + 2 \Delta I_A^b) \quad (14)$$

The pixel q will be classified as a contour pixel if all values of $S(q, p')$ are greater than $S(q, p)$ and then $\Delta S > 0$.

As $d_A > 0$, it is sufficient to have:

$2d_B + 2d_b - d_A - 2 \Delta I_A^b > 0$ and $2d_b - d_A + 2 \Delta I_A^b < 0$, this implies:

$$2d_b + 2 \Delta I_A^b < d_A < 2d_B + 2d_b - 2 \Delta I_A^b \quad (15)$$

The same reasoning is applied for other combination of positions of $I_A^b, I_B^b, I_A^f, I_B^f$, we found:

- if $I_A^b < I_B^b < I_A^f < I_B^f$, $\Delta S > 0$ if $d_A > 2d_b + 2 \Delta I_A^b$, $d_A < 2d_b + 2d_B$.

-if $I_B^b < I_A^b < I_B^f < I_A^f$, $\Delta S > 0$ if $d_A < 2d_b + 2d_B - 2 \Delta I_A^b$, ($d_A > 2d_b$ is verified)

- if $I_B^b < I_A^b < I_A^f < I_B^f$, $\Delta S > 0$ if $d_A < 2d_b + 2d_B$, ($d_A > 2d_b$ is verified)

Secondly, we assume that $d_A < 0$, we obtain:

- if $I_A^f < I_B^f < I_B^b < I_A^b$: $\Delta S > 0$ if $d_A < 2d_b - 2 \Delta I_A^b$, $d_A > 2d_B + 2d_b + 2 \Delta I_A^b$.

- if $I_B^f < I_A^f < I_B^b < I_A^b$: $\Delta S > 0$ if $d_A < 2d_b - 2 \Delta I_A^b$, $d_A > 2d_B + 2d_b$.

- if $I_A^f < I_B^f < I_A^b < I_B^b$: $\Delta S > 0$ if $d_A > 2d_B + 2d_b + 2 \Delta I_A^b$, ($d_A < 2d_b$ is verified).

- if $I_B^f < I_A^f < I_A^b < I_B^b$: $\Delta S > 0$ if $d_A > 2d_B + 2d_b$, ($d_A < 2d_b$ is verified)

References

- [1] S. Arya, D. M. Mount, N. S. Netanyahu, R. Silverman and A. Y. Wu, An optimal algorithm for approximate nearest neighbor searching fixed dimensions, *J. ACM*, Vol. 45(6), pp. 891-923, 1998
- [2] S. Arya and D. M. Mount, Approximate range searching, *Computational Geometry*, Vol. 17, N 3-4, pp 135-152, 2000
- [3] P. Arbelaez, M. Maire, C. Fowlkes and J. Malik, Contour Detection and Hierarchical Image Segmentation, *IEEE Transactions on Pattern Analysis and Machine Intelligence*, Vol. 33(5), pp. 898-916, May 2011
- [4] M. Ashikhmin, Synthesizing Natural Textures, *Proceedings of 2001 ACM Symposium on Interactive 3D Graphics, I3D'2001*, ACM Press, pp. 217-226, 2001
- [5] M. Ashikhmin, Fast texture transfer, *IEEE Computer Graphics and Applications*, Vol. 23(4), pp. 38-43, 2003
- [6] P. Bhat, S. Ingram and G. Turk, Geometric texture synthesis by example, *Proceedings of the 2004 Eurographics/ACM SIGGRAPH symposium on Geometry processing, SGP '04*, pp. 41-44, 2004, Nice, France
- [7] E. Borenstein and S. Ullman, Classic-specific, top-down segmentation. In *ECCV*, Copenhagen, Vol. 2, pp. 109-124, 2002
- [8] E. Borenstein, E. Sharon and S. Ullman, Combining Top-down and Bottom-up Segmentation, *IEEE Transactions on Pattern Analysis and Machine Intelligence*, 30(12), pp. 2109-2125, 2008
- [9] J. Canny, A computational approach to edge detection, *PAMI*, 1986.
- [10] V. Caselles, R. Kimmel, G. Sapiro, Geodesic active contours. *International Journal of Computer Vision*, 22(1), pp. 6179, 1997.
- [11] Caviar, EC Funded CAVIAR project/IST 2001 37540, Benchmark Data, 2001
- [12] L. Cheng, S. Vishwanathan and X. Zhang, Consistent image analogies using semi-supervised learning, *IEEE Conference on Computer Vision and Pattern Recognition (CVPR)*, Anchorage, AK, 2008

- [13] E. Chuang, D. Sher, X two test for feature detection, PR 26 (11) (1993) 16711681.
- [14] L. Cohen, I. Cohen, Finite element methods for active contour models and balloons for 2-D and 3-D images. IEEE Transactions on Pattern Analysis and Machine Intelligence, 15(11), pp. 11311147, 1993.
- [15] J. S. De Bonet, Multiresolution sampling procedure for analysis and synthesis of texture images, Proceedings of the 24th annual conference on Computer graphics and interactive techniques, SIGGRAPH '97, pp. 361–368, 1997
- [16] J. DeWinter and J. Wagemans, Segmentation of object outlines into parts: A large-scale integrative study, Cognition, Vol. 99(3), pp. 275 - 325, 2006
- [17] M. Donoser, H. Riemenschneider and H. Bischof, Linked Edges as Stable Region Boundaries”, Proceedings of Conference on Computer Vision and Pattern Recognition (CVPR), 2010
- [18] R. O. Duda and P. E. Hart, Pattern Classification and Scene Analysis, New York: Wiley, 1973
- [19] A. A. Efros and T. K. Leung, Texture Synthesis by Non-Parametric Sampling, IEEE International Conference on Computer Vision, Vol. 2, 1999
- [20] F. J. Estrada and A. D. Jepson, Robust Boundary Detection With Adaptive Grouping, Conference on Computer Vision and Pattern Recognition Workshop, 2006. CVPRW '06
- [21] W. T. Freeman, E. C. Pasztor, O. T. Carmichael, Learning Low-Level Vision, International Journal of Computer Vision 40(1), pp. 25-47, 2000
- [22] W. T. Freeman and E. H. Adelson, The design and use of steerable filters, PAMI, 1991.
- [23] J. Freixenet, X. Munoz, D. Raba, J. Marti and X. Cufi, Yet Another Survey on Image Segmentation: Region and Boundary Information Integration, ECCV (3), pp. 408-422, 2002

- [24] L. He, Z. Peng, B. Everding, X. Wang, C. Y. Han, K. L. Weiss, W. G. Wee, A comparative study of deformable contour methods on medical image segmentation. *Image and Vision Computing* 26 (2008), pp. 141163
- [25] D. J. Heeger and J. R. Bergen, Pyramid-based texture analysis/synthesis, *Proceedings of the 22nd annual conference on Computer graphics and interactive techniques, SIGGRAPH '95*, pp. 229-238, New York, NY, USA, 1995
- [26] A. Hertzmann, C. E. Jacobs, N. Oliver, B. Curless and D. H. Salesin, Image analogies, *Proceedings of the 28th annual ACM conference on Computer graphics and interactive techniques, SIGGRAPH '01*, pp. 327-340, New York, NY, USA
- [27] A. Hertzmann, N. Oliver, B. Curless, S. M. Seitz, *Curve Analogies, EGRW '02 Proceedings of the 13th Eurographics workshop on Rendering Switzerland, Switzerland, 2002*
- [28] J.S.Huang, D.H. Tseng, *Statistical theory of edge detection, CGIP* 43 (1988) 337346.
- [29] (1) M. Kass, A. Witkin, D. Terzopoulos, Snakes: active contour models, *International Journal of Computer Vision*, 1(4), pp. 321331, 1988.
- [30] P. Kovesei, Image features from phase congruency, *Videre: J. Comp. Vis. Res.* 1 (3)(1999).
- [31] J. B. Lackey and M. D. Colagrosso, Supervised Segmentation of Visible Human Data with Image Analogies, *IC-AI*, pp 843-847, 2004
- [32] M. Maire, P. Arbelaez, C. Fowlkes, and J. Malik. Using contours to detect and localize junctions in natural images. In *CVPR*, pages 18, 2008.
- [33] R. Malladi, J. Sethian, B. Vemuri, Shape modeling with front propagation, *IEEE Transactions on Pattern Analysis and Machine Intelligence*, 17(2), pp. 158171, 1995.
- [34] D. C. Marr and E. Hildreth, Theory of edge detection, *Proceedings of the Royal Society of London*, 1980

- [35] D.R. Martin, C. Fowlkes, and M. Jitendra, Learning to Detect Natural Image Boundaries Using Local Brightness, Color, and Texture Cues, *IEEE Trans. Pattern Anal. Mach. Intell.* Vol. 26(5), 2004, pp. 530-549,
- [36] T. McInerney, D. Terzopoulos, T-snakes: topologically adaptive snakes. *Medical Image Analysis*, 4(2), pp. 7391, 2000.
- [37] M. C. Morrone and R. Owens, Feature detection from local energy, *Pattern Recognition Letters*, 1987.
- [38] G. Papari and N. Petkov, Edge and line oriented contour detection: State of the art, *Image Vision Computing Journal*, Vol. 29(2-3), pp. 79-103, 2011
- [39] N. Payet, S. Todorovic, SLEDGE: Sequential Labeling of Image Edges for Boundary Detection, *International Journal of Computer Vision* (2013) 104:15-37
- [40] P. Perona and J. Malik, Detecting and localizing edges composed of steps, peaks and roofs, *ICCV*, 1990.
- [41] Pets 2009, PETS 2009 Benchmark Data, University of Reading, UK, 2009,
- [42] J. M. S. Prewitt, Object enhancement and extraction, *Processing and Psychopictorics*, B. Lipkin and A. Rosenfeld. Eds. Academic Press, New York, 1970
- [43] D. Reisfeld, The constrained phase congruency feature detector: simultaneous localization, classification and scale determination, *Pattern Recognition Letters*, 17 (11) (1996) 11611169.
- [44] B. Robbins, R. Owens, 2d feature detection via local energy, *IVC* 15 (5) (1997), pp. 353368.
- [45] L. G. Roberts, Machine perception of three-dimensional solids, *Optical and Electro-Optical Information Processing*, J. T. Tippett et al. Eds. Cambridge, MA: MIT Press, 1965
- [46] C. Ronse, On idempotence and related requirements in edge detection, *IEEE TPAMI*, 15 (5) (1993) 484491.
- [47] M.A. Ruzon, C. Tomasi, Edge, junction, and corner detection using color distributions, *IEEE T-PAMI* 23 (11) (2001) 12811295.

- [48] J. S. Suri, K. Liu, S. Singh, S. N. Laxminarayan, X. Zeng and L. Reden, Shape recovery algorithms using level sets in 2-D/3-D medical imagery: a state-of-the-art review, *IEEE Transactions on Information Technology in Biomedicine*, Vol. 6(1), pp. 8-28, 2002
- [49] D. Sykora, J. Burianek and J. Zara, Unsupervised colorization of black-and-white cartoons, *Proceedings of the 3rd international symposium on Non-photorealistic animation and rendering, NPAR '04*, pp. 121-127, 2004, Annecy, France
- [50] S. Venkatesh, R. Owens, On the classification of image features, *Pattern Recognition Letters*, 11 (5) (1990), pp. 339349.
- [51] G. Wang, T. Wong and P. Heng, Deringing cartoons by image analogies, *ACM Trans. Graph*, Vol. 25(20), pp 1360-1379, October 2006
- [52] B. Wandell, *Foundations of Vision*, Sinauer Associates Inc., 1995
- [53] C. Xu, J. Prince, Snakes, shapes, and gradient vector flow. *IEEE Transactions on Image Processing*, 7 (3), pp. 359369, 1998.
- [54] C. Zhang, X. Li, X. Ruan, Y. Zhao, M. Yang, Discriminative Generative Contour Detection, In the proceedings of BMVC, 2013
- [55] D. Ziou and S. Tabbone, *Edge Detection Techniques - An Overview*, *International Journal of Pattern Recognition and Artificial Intelligence*, 1998